Quasi-Analytical Modeling of Transmission/Reflection in Strip/Slit Gratings Loaded With Dielectric Slabs

Raúl Rodríguez-Berral, Francisco Medina, *Fellow, IEEE*, Francisco Mesa, *Senior Member, IEEE*, and María García-Vigueras, *Student Member, IEEE*

***Abstract*—This paper presents a quasi-analytical approach to study the classic topic of transmission/reflection of electromagnetic waves through 1-D periodic arrays of strips/slits in metal screens. The approach is based on standard waveguide discontinuity theory. Starting from field equations, it is inferred a circuit-like reduced-order model with just one parameter to be determined. The value of this parameter can be obtained from the transmission/reflection coefficient provided by any full-wave method at just one single frequency. In this way, the computation effort to obtain very wide-band responses of periodically distributed slits or strips under oblique TE/TM illumination in the presence of loading dielectric slabs is reduced to the full-wave analysis of the structure at a single frequency value. For relatively narrow strip/slit gratings, this procedure gives very accurate results even for very complicated transmission/reflection spectra. An additional advantage of the present approach is that it allows for an easy understanding of the underlying physics of the phenomena involved.**

***Index Terms*—Diffraction gratings, equivalent-circuit model, extraordinary and conventional transmission/reflection, impedance matching.**

I. Introduction

THE study of the transmissivity/reflectivity through/from periodically structured metal surfaces has been a topic of intense research activity for decades. The study of optical gratings is a well-known example of this classical research activity [1]–[4]. More recently, a huge interest on the study of these periodic structures has flourished in connection with the discovery of the extraordinary optical transmission (EOT) phenomenon [5]. Since then, hundreds of papers have been published on the topic and, nowadays, EOT is quite well understood (see, for instance, a number of comprehensive and authoritative reviews in [6]–[11]). A point of view on EOT alternative to the widely accepted theory of the interaction of the impinging wave with surface waves supported by the periodic structure was reported in [12]. In this latter work, the electrically small aperture involved in the process is seen as a reactive discontinuity in the path of an electromagnetic mode propagating along a waveguide. The waveguide can be a real waveguide, such as the circular-section waveguide considered in [13] and [14], or a virtual waveguide accounting for each of the unit cells of the periodically perforated screen [12], [15], [16]. This point of view is very fruitful because it leads straightforwardly to a circuit-like model having just a few parameters to be determined. Models of this type have been successfully adapted to various structures, such as simple and compound slit gratings [17]. Note that once the parameters of the circuit model are known, the transmission and reflection coefficients of the structure can be accurately generated for a very wide frequency range, thus avoiding lengthy calculations. Apart from the computational advantage, the qualitative response of the system can easily be anticipated from simple circuit-theory-based reasoning.

Many analytical approaches proposed to study the above structures have been restricted to free-standing metal structures. The presence of dielectric slabs to mechanically support the patterned metal surface, although not always mandatory, is often required. Furthermore, dielectric slab manipulation can give the designer additional control on the transmission/reflection properties of the periodic structure. Due to this reason, some authors have paid attention to the analysis of metallic perforated screens printed on dielectric slabs [18]–[21]. The presence of the dielectric slabs makes the transmission spectrum much richer than that of the free-standing structures. Hence, periodically patterned metallic structures printed on dielectric substrates have been of common use in microwave and antenna engineering: these are the so-called frequency selective surfaces (FSSs). This kind of filtering structure has exhaustively been studied for many years. The essentials of their history, performance, and design techniques can be found in a well-known textbook [22]. In the microwaves and antennas literature, most of the attention has been paid to the study of what it might be called *conventional* transmissivity/reflectivity. This can be motivated by the search for practical engineering applications rather than new electromagnetic effects. Nevertheless, the tools developed for the fast analysis and design of conventional FSSs (namely, circuit modeling techniques) could be adapted to account for the exotic phenomena that attract the attention of physicists and experts in optics.

Manuscript received June 07, 2011; revised December 08, 2011; accepted December 14, 2011. Date of publication January 31, 2012; date of current version March 02, 2012. This work has been supported by the Spanish Ministerio de Ciencia e Innovación and European Union FEDER funds (projects TEC2010-16948 and TEC2010-21520-C04-04), by Junta de Andalucía (project TIC–4595), and Regional Seneca project 08833/PI/08 (Regional Scholarship PMPDI-UPCT-2009).

R. Rodríguez-Berral and F. Mesa are with the Microwaves Group, Department of Applied Physics 1, ETS de Ingeniería Informática, University of Seville, 41012-Seville, Spain (e-mail: rrberral@us.es; mesa@us.es).

F. Medina is with the Department of Electronics and Electromagnetism, Faculty of Physics, University of Seville, 41012-Seville, Spain (e-mail: medina@us.es).

M. García-Vigueras is with Departamento de las Tecnologías de la Información y las Comunicaciones. Universidad Politécnica de Cartagena, 30202 Murcia, Spain (e-mail: maria.garcia@upct.es).

Color versions of one or more of the figures in this paper are available online at http://ieeexplore.ieee.org.

Digital Object Identifier 10.1109/TMTT.2011.2181186

0018-9480/$31.00 © 2012 IEEE

Authorized licensed use limited to: Universidad de Sevilla. Downloaded on June 03,2020 at 14:46:29 UTC from IEEE Xplore. Restrictions apply.

The use of circuit models to deal with the electromagnetic behavior of periodic metallic, dielectric or metalo-dielectric structures has a long tradition. Circuit models were widely used to explain the filtering properties of 2-D diffraction grids employed in the design of infrared filters [23]–[25]. The same methodology can also be applied in other frequency ranges (see, for instance, [26]–[30], among many other papers). However, the circuit models proposed in the literature are often limited to frequencies significantly below the onset of the grating lobes of the periodic structure, which means that the unit-cell dimensions are smaller than the operating wavelength. This is an important drawback to explore the part of the frequency spectrum that exhibits exotic characteristics. Moreover, no systematic method is usually provided to build the circuit topology and to compute the circuit parameters. Thus, most of the available circuit models fail when dealing with relatively complex phenomena, such as extraordinary transmission or complex transmission spectra caused by the interaction of higher order modes. Due to this, it is important to develop new strategies to efficiently deal with this problem. In this way, a very accurate circuit model that incorporates some closed-form frequency-dependent components and transmission lines has been reported in [31] for the modeling of 2-D arrays of dipoles sandwiched between dielectric slabs. The problem of arrays of infinitely long narrow slits made in metal screens has recently been solved in [32] for the special case of TM normal incidence. In [33] and [34], a similar model has also been used to deal with the so-called anomalous extraordinary transmission of a periodic 2-D structure.

The purpose of the present work is then to extend the heuristic approach presented in [32]–[34] in order to provide a more rigorous analytical basis to account for a number of new situations for narrow slit/strip systems sandwiched between different dielectric slabs under oblique incidence and TM/TE polarizations. Particular cases of the general situations to be considered in this work are shown in Fig. 1. In the notation employed for the specific layered media in this figure, it has been considered that medium (1) is the first dielectric slab found by the impinging wave coming from the free-space left hand side (free space will always be denoted by superscript (0)). The following dielectric slabs are denoted by superscript (i), with $i = 2, 3, \ldots$. The case of slits/strips placed in the boundary between two semi-infinite media was studied in two classical papers by Guglielmi and Oliner [35], [36]. Unfortunately, the presence of dielectric slabs was not considered in the methodology reported in [35] and [36]. Now, our proposed technique provides a suitable circuit model for a very general situation with just one parameter to be numerically calculated. This parameter could eventually be known in closed form or, in general, extracted from one value of the scattering parameters computed at one specific frequency point (a method-of-moment scheme is used in this paper for this purpose). A number of examples will illustrate how our simple equivalent-circuit model accounts for the most fine details of the complex transmission/reflection spectra exhibited by this kind of lamellar gratings. The limits of validity of our model are also discussed.

II. Statement of the Problem and Theoretical Basis

In this section, we investigate the nature of the circuit models accounting for the physical situations depicted in Fig. 1. An

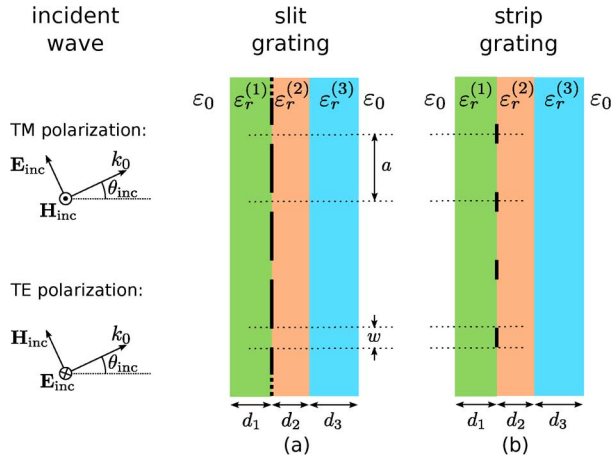

Fig. 1. Structures under study. (a) Slit grating consisting of a periodic distribution of relatively narrow slits made in a thin metal sheet embedded in a stratified dielectric medium. (b) Strip grating, similar to (a) but with narrow strips instead of narrow slits. The structures are illuminated with uniform TEM waves with an arbitrary angle of incidence.

infinitely thin metallic screen periodically perforated with slits (slit grating) and sandwiched between two different layered dielectric media is depicted in Fig. 1(a). The quasi-dual structure consisting of an array of parallel metal strips placed in a similar dielectric environment is considered in Fig. 1(b). A TM- or TE-polarized plane wave impinges on any of these structures. If the metal is removed, the incident wave would partially be reflected and transmitted through every interface between the dielectric layers. As is well known, this last problem can be studied in terms of an analogous transmission line network in which each dielectric layer is represented by a length of transmission line whose characteristic impedance is given by the wave impedance inside the layer [37]. The presence of the periodic metallic pattern can be accounted for by adding appropriate circuit elements to this basic transmission line background. Although there are many different circuits that could fit the experimental or numerically obtained reflection/transmission curves, an appropriate choice based on physical and/or mathematical considerations is key to keep the number of parameters as small as possible while yielding very good accuracy in a wide frequency band. Thus, in this section, we provide the theoretical foundation for the proposed circuit models for the situations depicted in Fig. 1. Under the assumption of electrically narrow slits/strips (or equivalently wide strips/slots), the topology of the appropriate equivalent circuits that account for the presence of metal strips/slits is easily inferred from the field equations at both sides of the discontinuity. For the sake of clarity, the derivation is first presented in detail for the case of normal incidence. Once the circuit models are obtained for this case, it is shown how they can be straightforwardly extended to the general case of oblique incidence.

Due to the periodic nature of the structure and the excitation, the problem can be reduced to the study of a single unit cell. Taking into account the symmetries of the structure, the unit cell is equivalent to a parallel-plate waveguide with electric/magnetic walls for normal TM/TE polarization of the incident wave. Inside the equivalent waveguide the screen acts as a capacitive/inductive iris discontinuity. This discontinuity

Authorized licensed use limited to: Universidad de Sevilla. Downloaded on June 03,2020 at 14:46:29 UTC from IEEE Xplore. Restrictions apply.

launches higher order modes that are coupled between themselves and with the incident field. Since modes of different order only couple mutually at the screen and not at the dielectric interfaces, our initial goal in next section will be to find the equivalent circuit that models the behavior of an iris discontinuity between two parallel-plate waveguides filled with different homogeneous dielectric slabs.

A. Narrow Slits, Normal Incidence

The unit cell problem under consideration is shown in Fig. 2. Due to the invariance of the problem along the direction of the slits (y), the TM/TE incident wave only excites TM/TE modes at the iris plane [TM: (E_x, H_y), TE: (E_y, H_x)]. For both TM and TE excitations, the corresponding transverse (to z) component of the electric field at both sides of the discontinuity can be expressed in terms of its modal expansion at $z = 0$ as (an implicit time dependence of the type $\exp(\mathrm{j}\omega t)$ is assumed and suppressed throughout the ongoing derivations)

$$E^{(1)}(x) = 1 + R + \sum_{n=1}^{\infty} E_n^{(1)} \cos(k_n x) \tag{1}$$

$$E^{(2)}(x) = T + \sum_{n=1}^{\infty} E_n^{(2)} \cos(k_n x) \tag{2}$$

where superscript (i), $i = 1, 2$ refers to region i (see Fig. 2), R and T are the reflection and transmission coefficients, respectively (an incident TEM wave with unit amplitude electric field has been considered), and $k_n = 2\pi n/a$ is the transverse modal wavenumber of the nth higher order mode. Similarly, the corresponding transverse magnetic field is given by

$$H^{(1)}(x) = Y_0^{(1)}(1 - R) - \sum_{n=1}^{\infty} Y_n^{(1)} E_n^{(1)} \cos(k_n x) \tag{3}$$

$$H^{(2)}(x) = Y_0^{(2)} T + \sum_{n=1}^{\infty} Y_n^{(2)} E_n^{(2)} \cos(k_n x) \tag{4}$$

where $Y_n^{(i)}$ is the following modal admittance of the nth mode in region i:

$$Y_n^{(i)} = \frac{1}{\eta^{(i)}} \begin{cases} k^{(i)}/\beta_n^{(i)}, & \text{TM modes} \\ \beta_n^{(i)}/k^{(i)}, & \text{TE modes} \end{cases} \tag{5}$$

with

$$\beta_n^{(i)} = \sqrt{\left(k^{(i)}\right)^2 - k_n^2} \tag{6}$$

being the longitudinal wavenumber of mode n in region i and

$$k^{(i)} = k_0 \sqrt{\varepsilon_r^{(i)}}, \quad \eta^{(i)} = \sqrt{\frac{\mu_0}{\varepsilon_0 \varepsilon_r^{(i)}}} = \frac{\eta_0}{\sqrt{\varepsilon_r^{(i)}}} \tag{7}$$

the intrinsic wavenumber and impedance of the dielectric medium in region i, respectively.

The transverse electric field must be zero on the perfect conductor screen and continuous across the slit region. Therefore, the transverse component of the electric field satisfies

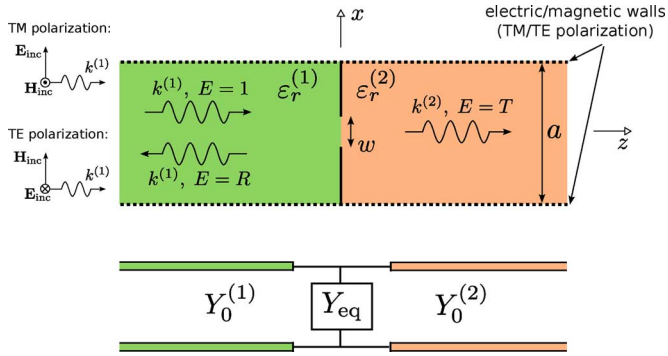

Fig. 2. Representation of the basic unit cell problems to be solved for normal incidence of TM/TE waves on a slit-like grating system. The top and bottom plane surfaces defining the generalized parallel plate waveguide will be perfect electric/magnetic walls for TM/TE waves. A general circuit valid for calculating the scattering parameters of the fundamental TEM mode is given at the bottom of the figure.

$E^{(1)}(x) = E^{(2)}(x)$ for all values of x. Hence, the coefficients of their modal expansions have to be equal, namely,

$$1 + R = T \tag{8}$$

$$E_n^{(1)} = E_n^{(2)}. \tag{9}$$

Note that (8) represents the continuity of the voltage in the transmission line model. Next we examine the projection of the tangential electric field over the modal profiles, given by the following integral:

$$\int_{-a/2}^{a/2} \cos(k_n x) E^{(i)}(x) \mathrm{d}x. \tag{10}$$

Due to the perfect conductor boundary condition on the metallic region, the integrand in (10) is nonzero only in the slit region $(|x| < w/2)$. Also, for narrow slits $(w \ll a)$ and not very high values of n, the cosine profile is approximately constant and equal to unity over the slit. Taking these facts into account, we have

$$\int_{-a/2}^{a/2} \cos(k_n x) E^{(i)}(x) \mathrm{d}x \approx \int_{-a/2}^{a/2} E^{(i)}(x) \mathrm{d}x. \tag{11}$$

Introducing the modal expansion (1) in (11), it is obtained the following relation between the TEM and the higher order coefficients:

$$E_n^{(i)} \approx 2(1 + R), \quad i = 1, 2. \tag{12}$$

Introducing now this approximation (valid in the narrow slit limit) into (3) and (4), and enforcing the continuity of the magnetic field across the slit $(|x| < w/2)$, it is obtained that

$$Y_0^{(1)}(1 - R) - 2(1 + R) \sum_{n=1}^{\infty} Y_n^{(1)} \cos(k_n x) = Y_0^{(2)}(1 + R) + 2(1 + R) \sum_{n=1}^{\infty} Y_n^{(2)} \cos(k_n x). \tag{13}$$

Authorized licensed use limited to: Universidad de Sevilla. Downloaded on June 03,2020 at 14:46:29 UTC from IEEE Xplore. Restrictions apply.

Enforcing a point matching condition at $x = 0$, (13) leads to the following expression for the reflection coefficient:

$$R = \frac{Y_0^{(1)} - Y_0^{(2)} - \sum_{n=1}^{\infty} 2\left(Y_n^{(1)} + Y_n^{(2)}\right)}{Y_0^{(1)} + Y_0^{(2)} + \sum_{n=1}^{\infty} 2\left(Y_n^{(1)} + Y_n^{(2)}\right)}. \quad (14)$$

If the global admittance of the equivalent circuit that would account for the scattered higher order modes in Fig. 2 is denoted as $Y_{\rm eq}$, basic transmission line theory tell us that the reflection coefficient is given by

$$R = \frac{Y_0^{(1)} - Y_0^{(2)} - Y_{\rm eq}}{Y_0^{(1)} + Y_0^{(2)} + Y_{\rm eq}}. \quad (15)$$

Comparing (14) and (15), the admittance of the equivalent circuit can be identified as

$$Y_{\rm eq} = \sum_{n=1}^{\infty} 2\left(Y_n^{(1)} + Y_n^{(2)}\right) \quad (16)$$

which clearly suggests an equivalent circuit that consists of a simple parallel connection of the modal admittances of the higher order modes, multiplied by two.

Although the above derivation is basically correct, there are some nuances that need further discussion. The approximation $\cos(k_n x) \approx 1$ [and also (12)] is accurate provided that $nw/a \ll 1$. As a consequence, we cannot retain a high number of higher order modes in the sums in (13), (14), and (16). In fact, for TE modes, it is found that $Y_n^{(i)} \sim n$ for $n \gg 1$, which would make (16) divergent. We could simply truncate the above series at some suitable value of n, but although this strategy can provide accurate results, it is not useful in practice due to its instability and the difficulty in finding a general criterion for the number of terms to be retained in each specific case. Fortunately, the contribution of these "problematic" higher order modes can easily be taken into account in an alternative way, resulting in a much more stable and reliable model, as explained next.

The contribution of modes with very high order gives rise to a strongly evanescent reactive field, confined in the close vicinity of the screen. As such, it seems reasonable to model the effect of this field as a given capacitance/inductance for TM/TE polarization. The mathematical reason for that comes from the frequency behavior of the modal admittances $Y_n^{(i)}$ in (5), which can be written as

$$Y_n^{(i)} = \frac{\rm j}{\eta^{(i)}} \begin{cases} \dfrac{f/f_n^{(i)}}{\sqrt{1-\left(f/f_n^{(i)}\right)^2}}, & \text{TM modes} \\ -\dfrac{\sqrt{1-\left(f/f_n^{(i)}\right)^2}}{f/f_n^{(i)}}, & \text{TE modes} \end{cases} \quad (17)$$

where f is the operating frequency and

$$f_n^{(i)} = n\frac{c}{a\sqrt{\varepsilon_r^{(i)}}} \quad (18)$$

is the cutoff frequency of mode n in region i (c is the speed of light in vacuum). If the operating frequency is much lower than the cutoff frequency of the first higher order mode, then all the modal admittances in (17) are positive (negative) imaginary quantities and approximately proportional to $f(f^{-1})$ for TM (TE) modes. Hence, the global effect of the discontinuity can appropriately be accounted for by a frequency-independent capacitance/inductance for TM/TE polarization. However, as frequency increases, the *lowest* higher order modes get close to their cutoff frequency (and eventually become propagative) and, thus, the full frequency dependence of their admittances given in (5) or (17) must be taken into account. However, the *remaining* higher order modes are still far below their cutoff frequency and their global contribution can still be described, to a good approximation, by a single frequency-independent capacitance/inductance. It is worth mentioning that the basic idea of the separation of the contribution of propagative and evanescent modes has been extensively used in the study of waveguides and free-standing gratings [38]–[40].

According to the above discussion and the parallel connection already inferred, the equivalent admittance of our proposed circuit can be written as

$$Y_{\rm eq} = \sum_{n=1}^{N} 2\left(Y_n^{(1)} + Y_n^{(2)}\right) + \begin{cases} {\rm j}\omega C_{\rm ho}, & \text{TM} \\ 1/{\rm j}\omega L_{\rm ho}, & \text{TE} \end{cases} \quad (19)$$

where there is only one parameter to be determined, namely, $C_{\rm ho}$ for TM and $L_{\rm ho}$ for TE polarization. It should be emphasized that this model has neither been proposed heuristically nor is based on qualitative reasoning. Rather, it has been deduced as a valid approximation following a rigorous procedure based on the continuity of the fields and the appropriate boundary conditions at the screen. The equivalent admittance in (19) is clearly formed by a parallel connection of $2N$ admittances whose values are twice the modal admittances of the first N higher order modes at both sides of the discontinuity together with a global capacitance/inductance accounting for the contribution of the infinite set of remaining TM/TE higher order modes. In most practical situations, the required N is very low, as it will be shown later. Here, it is important to note that the modal admittances at both sides of the screen appear in the model multiplied by the same factor. This might seem surprising since the screen is surrounded by different dielectric media, and hence it could be expected that the factors accompanying both admittances were different (in other words, these factors could be expected to depend on the permittivity of the dielectric medium). However, the derivation of the equivalent circuit suggests that these factors are not different because they are related to the vertical (x) modal profiles, which clearly do not depend on the permittivity of the medium but only on the order of the mode and the size of the waveguide.

B. Narrow Strips, Normal Incidence

For the narrow strip limit, the situation to be considered is depicted in Fig. 3 (strip-like grating). Here, we use the modal expansion of the fields already proposed in (1)–(4), the relations (8) and (9), and consider the following projection of the magnetic field discontinuity over the cosine profiles:

$$\int_{-a/2}^{a/2} \cos(k_n x)\left[H^{(2)}(x) - H^{(1)}(x)\right] {\rm d}x. \quad (20)$$

Authorized licensed use limited to: Universidad de Sevilla. Downloaded on June 03,2020 at 14:46:29 UTC from IEEE Xplore. Restrictions apply.

Similar to (10), the integrand of (20) is zero for $|x| > w/2$. Also, for narrow strips and not very high values of n, the cosines can be approximated by unity for $|x| < w/2$, obtaining

$$\int_{-a/2}^{a/2} \cos(k_n x)\left[H^{(2)}(x) - H^{(1)}(x)\right] \mathrm{d}x \approx \int_{-a/2}^{a/2} \left[H^{(2)}(x) - H^{(1)}(x)\right] \mathrm{d}x. \quad (21)$$

Using (3), (4), (8), and (9) in (21), it is obtained that

$$E_n^{(1)} \approx \frac{2}{Y_n^{(1)} + Y_n^{(2)}} \left[R\left(Y_0^{(1)} + Y_0^{(2)}\right) - Y_0^{(1)} + Y_0^{(2)}\right]. \quad (22)$$

Taking into account the boundary condition for the electric field on the strip surface

$$E^{(1)}(x) = 0; \quad |x| < \frac{w}{2} \quad (23)$$

and making use of (1) and (22), we have

$$1 + R + \left[R\left(Y_0^{(1)} + Y_0^{(2)}\right) - Y_0^{(1)} + Y_0^{(2)}\right] \times \sum_{n=1}^{\infty} \frac{2}{Y_n^{(1)} + Y_n^{(2)}} \cos(k_n x) = 0. \quad (24)$$

After enforcing a point matching condition at $x = 0$ in this last equation, the reflection coefficient can finally be written as

$$R \approx \frac{Y_0^{(1)} - Y_0^{(2)} - \left[\sum_{n=1}^{\infty} \frac{2}{Y_n^{(1)} + Y_n^{(2)}}\right]^{-1}}{Y_0^{(1)} + Y_0^{(2)} + \left[\sum_{n=1}^{\infty} \frac{2}{Y_n^{(1)} + Y_n^{(2)}}\right]^{-1}}. \quad (25)$$

Thus, the global impedance of the equivalent circuit is found to be

$$Z_{\mathrm{eq}} = \sum_{n=1}^{\infty} \frac{2}{Y_n^{(1)} + Y_n^{(2)}}. \quad (26)$$

Hence, the proposed equivalent impedance of the one-parameter circuit model for narrow strips is given by

$$Z_{\mathrm{eq}} = \sum_{n=1}^{N} \frac{2}{Y_n^{(1)} + Y_n^{(2)}} + \begin{cases} 1/\mathrm{j}\omega C_{\mathrm{ho}}, & \text{TM} \\ \mathrm{j}\omega L_{\mathrm{ho}}, & \text{TE}. \end{cases} \quad (27)$$

The equivalent circuit then consists of $N + 1$ series connected elements, N of which are shunt connections between the admittances of the nth higher order mode in regions 1 and 2, divided by two. The last series-connected component is a global capacitance or inductance accounting for the very high-order modes.

C. Generalization to Oblique Incidence

In the case of oblique incidence, the unit-cell problem to be considered consists of a discontinuity in a generalized parallel-plate waveguide with periodic boundary conditions (instead of electric or magnetic walls). The modal expansion of the fields

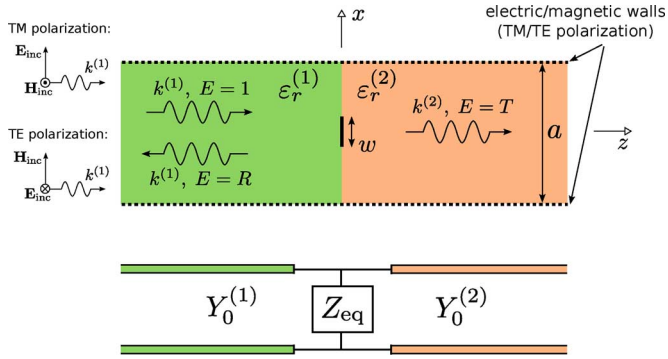

Fig. 3. Representation of the basic unit cell problems to be solved for normal incidence of TM/TE waves on a strip-like grating system. The top and bottom plane surfaces defining the generalized parallel plate waveguide will be perfect conductors for TM waves and perfect magnetic conductors for TE waves. A general circuit valid for calculating the scattering parameters of the fundamental TEM mode is given at the bottom of the figure.

at $z = 0$ is now a Floquet-series expansion. For each of the modes of the normal incidence case, we have now a pair of positive/negative order spatial harmonics, namely,

$$E^{(1)}(x) = \left\{1 + R + \sum_{n=1}^{\infty}\left[E_n^{(1)} \mathrm{e}^{-\mathrm{j}k_n x} + E_{-n}^{(1)} \mathrm{e}^{\mathrm{j}k_n x}\right]\right\} \mathrm{e}^{-\mathrm{j}k_t x} \quad (28)$$

$$E^{(2)}(x) = \left\{T + \sum_{n=1}^{\infty}\left[E_n^{(2)} \mathrm{e}^{-\mathrm{j}k_n x} + E_{-n}^{(2)} \mathrm{e}^{\mathrm{j}k_n x}\right]\right\} \mathrm{e}^{-\mathrm{j}k_t x} \quad (29)$$

and

$$H^{(1)}(x) = \left\{Y_0^{(1)}(1 - R) - \sum_{n=1}^{\infty}\left[Y_n^{(1)} E_n^{(1)} \mathrm{e}^{-\mathrm{j}k_n x} + Y_{-n}^{(1)} E_{-n}^{(1)} \mathrm{e}^{\mathrm{j}k_n x}\right]\right\} \mathrm{e}^{-\mathrm{j}k_t x} \quad (30)$$

$$H^{(2)}(x) = \left\{Y_0^{(2)} T + \sum_{n=1}^{\infty}\left[Y_n^{(2)} E_n^{(2)} \mathrm{e}^{-\mathrm{j}k_n x} + Y_{-n}^{(2)} E_{-n}^{(2)} \mathrm{e}^{\mathrm{j}k_n x}\right]\right\} \mathrm{e}^{-\mathrm{j}k_t x} \quad (31)$$

where

$$k_t = \phi/a = k^{(1)} \sin\theta_{\mathrm{inc}} \quad (32)$$

is the component of the incident wavevector tangential to the screen (ϕ is the phase shift impressed by the incident wave between adjacent unit cells). Each spatial harmonic plays the role of a mode of the unit-cell in the generalized waveguide problem, whose "modal" admittance $Y_{\pm n}^{(i)}$ can be computed from (5) with

$$\beta_{\pm n}^{(i)} = \sqrt{\left(k^{(i)}\right)^2 - (k_t \pm k_n)^2}. \quad (33)$$

The cutoff frequency of the $\pm n$ spatial harmonic in medium (i) $(i = 1, 2)$ is given by

$$f_{\pm n}^{(i)} = \frac{nc}{a} \frac{1}{\sqrt{\varepsilon_r^{(i)}} \mp \sqrt{\varepsilon_r^{(1)}} \sin\theta_{\mathrm{inc}}}. \quad (34)$$

Authorized licensed use limited to: Universidad de Sevilla. Downloaded on June 03,2020 at 14:46:29 UTC from IEEE Xplore. Restrictions apply.

and its "modal" transverse field profile is $\mathrm{e}^{-\mathrm{j}(k_t \pm k_n)x}$. Considering now that this transverse field profile can be approximated as

$$\mathrm{e}^{-\mathrm{j}(k_t \pm k_n)x} \approx 1, \quad \text{for } |x| < w/2 \text{ and } w \ll a \tag{35}$$

we obtain expressions completely analogous to the ones presented in the preceding two sections for the case of normal incidence. Thus, the following one-parameter equivalent admittance is obtained for the circuit model accounting for the narrow-slit case:

$$Y_{\mathrm{eq}} = \sum_{\substack{n=-N^- \\ n\neq 0}}^{N^+} \left(Y_n^{(1)} + Y_n^{(2)}\right) + \begin{cases} \mathrm{j}\omega C_{\mathrm{ho}}, & \text{TM} \\ 1/\mathrm{j}\omega L_{\mathrm{ho}}, & \text{TE} \end{cases} \tag{36}$$

whereas, for the narrow-strip case, we obtain

$$Z_{\mathrm{eq}} = \sum_{\substack{n=-N^- \\ n\neq 0}}^{N^+} \frac{1}{Y_n^{(1)} + Y_n^{(2)}} + \begin{cases} 1/\mathrm{j}\omega C_{\mathrm{ho}}, & \text{TM} \\ \mathrm{j}\omega L_{\mathrm{ho}}, & \text{TE.} \end{cases} \tag{37}$$

The corresponding equivalent circuits are similar to those obtained in previous sections, except for the factor 2 appearing in each term in (19) and (27), which is now absent. It makes the models for normal and oblique incidence mutually consistent, since as $\theta \to 0$, both $Y_{-n}^{(i)}$ and $Y_n^{(i)}$ tend to the corresponding modal admittance of the normal-incidence nth-order mode. Thus, the corresponding $+/-$ terms in (36) or (37) add together to yield one single term multiplied by the factor 2.

At this point, it should be noticed that the approximation $\cos(k_n w) \approx 1$ used to obtain the normal incidence models is correct up to the second order in $k_n w/2$, whereas $\exp[-\mathrm{j}(k_t \pm k_n)w] \approx 1$ is valid only up to first order. Therefore, it is expected that the range of validity of the circuit model for oblique incidence is more restricted. Nevertheless, even for oblique incidence, the proposed one-parameter models are found to be quite robust and provide accurate results for $w/\lambda_0 \lesssim 0.15$ and $w/a \lesssim 1/3$, which is remarkable.

D. Finite Thickness Dielectric Layers and Losses

The equivalent-circuit models developed in preceding sections account for the coupling of the different modes (or spatial harmonics) at the periodic screen sandwiched between semi-infinite dielectric media. If finite-thickness dielectric slabs are now incorporated in the analysis, it should be considered that each mode is also partially reflected and transmitted at each dielectric interface, without coupling with modes of different order. As commented above, the propagation of each mode through the dielectric slabs (and its transmission/reflection at the interfaces) can be rigorously described in terms of a transmission line network in which each dielectric layer is represented by a length of transmission line whose characteristic impedance is the modal impedance inside the corresponding dielectric medium. Therefore, the presence of the different dielectric slabs can be straightforwardly incorporated in the model by simply replacing the modal admittances in (19), (27), (36), and (37) with the input admittances of the corresponding transmission lines. Note that, in most practical cases, the incident wave comes from free-space, and thus the component of the incident wavevector tangential to the screen is $k_t = k_0 \sin(\theta_{\mathrm{inc}})$ (the expression given in (32) was for the

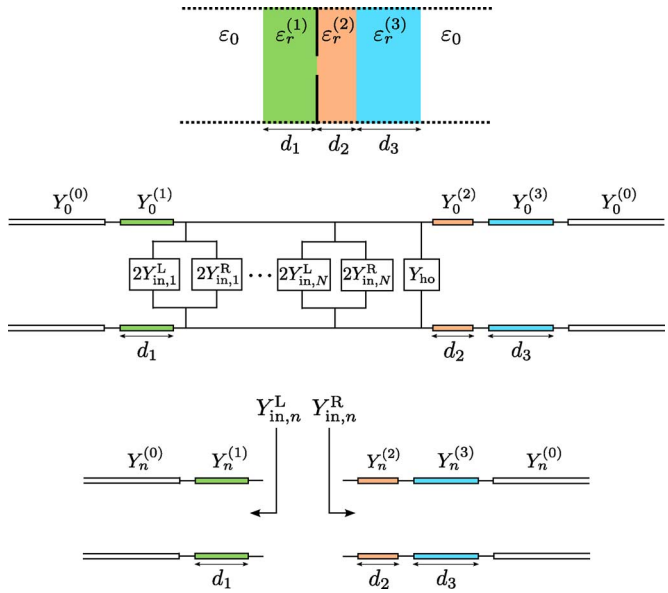

Fig. 4. Unit cell for a multilayer slit-like grating structure together with its equivalent circuit (see expression (36)). The definition of the required input admittances (for the right and left sides) can be deduced from the bottom circuits.

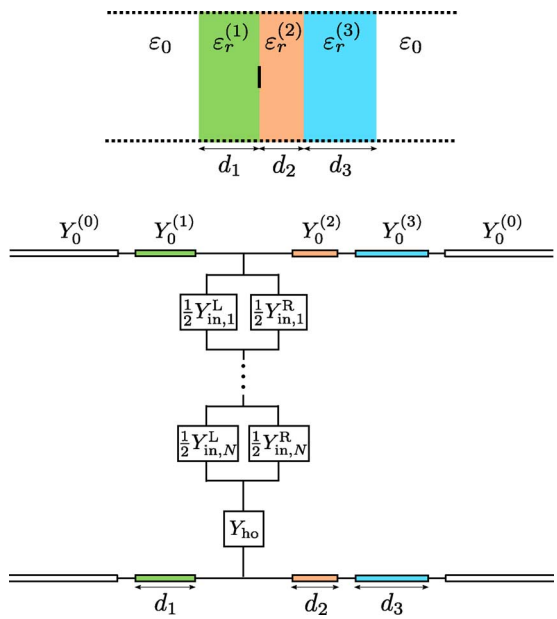

Fig. 5. Unit cell for a multilayer strip-like grating structure together with its equivalent circuit (see expression (37)). The input admittances (for the right and left sides) can be deduced from the bottom circuits in Fig. 4.

case of two semi-infinite dielectric media). As an example, Fig. 4 shows the model for normal incidence in the case of a slit grating sandwiched between a dielectric slab at the left-hand side and two dielectric slabs at the right-hand side. The strip grating version is depicted in Fig. 5.

When a higher order mode becomes propagative inside the dielectric layers, the corresponding input admittance may exhibit a complicated frequency behavior, including zeros, poles, and sign reversals. It may result in an equivalent admittance that behaves as a short/open circuit at given frequency values, and also in a change of its global reactive nature from capacitive to inductive, and vice versa. This rich frequency behavior is the reason for the transmission and reflection peaks introduced by

Authorized licensed use limited to: Universidad de Sevilla. Downloaded on June 03,2020 at 14:46:29 UTC from IEEE Xplore. Restrictions apply.

the presence of the dielectric slabs and, in general, for all the new phenomenology observed in the sophisticated spectra of these structures.

According to the above discussion, the number of terms whose complete frequency dependence must be taken into account (N for normal incidence and $N^+ + N^-$ for oblique incidence) in order to accurately reproduce the transmission behavior of the structure is determined by the number of higher order modes (or spatial harmonics) that become propagative inside the dielectric with the highest permittivity in the frequency range of interest. In addition, the first evanescent mode should also be included if its cutoff frequency is close to be reached. As a consequence, the number of terms in the equivalent circuits (lumped elements characterized by the input admittances shown in Figs. 4 and 5) is usually small for most practical cases. For an incident wave impinging from free space at an incidence angle $\theta_{\rm inc}$, the cutoff frequency of the $\pm n$ spatial harmonic inside an homogeneous dielectric layer with relative permittivity ε_r is given by

$$f_{\pm n} = \frac{nc}{a}\frac{1}{\sqrt{\varepsilon_r} \mp \sin\theta_{\rm inc}} \tag{38}$$

and thus the number of higher order modes whose cutoff frequencies inside this dielectric layer is below the onset of the first grating lobe is

$$N^{\pm} = \left\lfloor \frac{\sqrt{\varepsilon_r} \mp \sin\theta_{\rm inc}}{1 + |\sin\theta_{\rm inc}|} \right\rfloor \tag{39}$$

where $\lfloor\cdot\rfloor$ indicates the nearest smaller integer. Therefore, for most practical cases, one single mode ($N = 1$) is commonly enough for low permittivity slabs ($\varepsilon_r < 4$) whereas $N = 3, 4$ would generally suffice for high permittivity substrates.

Finally, dielectric losses can be taken into account by simply introducing the complex value of the permittivity

$$\varepsilon_r^{(i)}\left(1 - {\rm j}\tan\delta^{(i)}\right) \tag{40}$$

in the expressions of the modal wavenumbers and characteristic admittances.

E. Computation of the Circuit Parameters

The equivalent-circuit models reported in previous subsections have only one parameter to be determined. This quasi-static capacitance/inductance appearing in expressions (19), (27), (36), and (37) can be known in closed form in some limiting cases although, in general, it can be computed from a single full-wave numerical modeling of the structure under study. Different specific strategies can be followed to relate the circuit parameters to the full-wave results. In the following, it is briefly explained the strategy used in this work to obtain the numerical results presented in Section III.

Using a full-wave numerical technique, one can obtain the amplitude of the modal fields propagating to the left and to the right inside each dielectric layer for a given amplitude of the incident wave. (Here, our choice has been a method of moments using multiple basis functions that incorporate the edge singularities.) In order to obtain a simple linear relation between the full-wave data and the circuit parameters, we consider the reflection coefficient of the TEM wave (or the zeroth-order spatial harmonic in the case of oblique incidence) that propagates inside the dielectric layer just at the immediate left side of the screen ($z = 0^-$). This reflection coefficient is denoted as S'_{11} and, according to our models, can be obtained in terms of the admittances in the equivalent circuit as

$$S'_{11} = \frac{Y_0^{\rm L} - \left(Y_{{\rm in},0}^{\rm R} + Y_{\rm eq}\right)}{Y_0^{\rm L} + \left(Y_{{\rm in},0}^{\rm R} + Y_{\rm eq}\right)} \tag{41}$$

where $Y_0^{\rm L}$ is the TEM wave admittance inside the dielectric medium to the immediate left of the screen, $Y_{{\rm in},0}^{\rm R}$ is the input admittance of the TEM transmission line network at the right side of the screen, and $Y_{\rm eq}$ is the global equivalent admittance that accounts for the effect of the slit/strip discontinuity. From (41), this equivalent admittance can be expressed as

$$Y_{\rm eq} = Y_0^{\rm L}\frac{1 - S'_{11}}{1 + S'_{11}} - Y_{{\rm in},0}^{\rm R}. \tag{42}$$

For the case of narrow slits and TM normal incidence, after introducing the generalization of (19) to multiple dielectric layers into (42), it is found that

$${\rm j}\omega C_{\rm ho} = Y_0^{\rm L}\frac{1 - S'_{11}}{1 + S'_{11}} - Y_{{\rm in},0}^{\rm R} - \sum_{n=1}^{N} 2\left(Y_{{\rm in},n}^{\rm L} + Y_{{\rm in},n}^{\rm R}\right) \tag{43}$$

where $Y_{{\rm in},n}^{\rm L}$ and $Y_{{\rm in},n}^{\rm R}$ are the input admittances of the transmission line network corresponding to the nth higher order mode at the left- and right-hand sides of the screen, respectively. Given the value of S_{11} at one given frequency, the value of the $C_{\rm ho}$ parameter can readily be obtained from (43). In practice, it is recommended to compute S_{11} at a low-frequency value where the circuit model is virtually exact; specifically, we have used $f = 1$ GHz for a structure with $a = 5$ mm, which means $f \approx 0.017 f_1^{(0)}$, with the (0) superscript denoting vacuum.

III. Numerical Results and Discussion

In this section, we discuss the two main features of the quasi-analytical model here proposed: i) the numerical efficiency that is achieved by the combination of our equivalent-circuit model with a single full-wave computation to obtain even very complex spectra in a wide frequency band, and ii) the predictive ability of our approach, which provides us with information to qualitatively understand the details of the transmission/reflection spectra.

To start with, we consider the case of narrow strips printed on a dielectric slab under normal TM illumination. Fig. 6 shows the magnitude of the reflection coefficient for this situation. The results obtained for the strip grating without the slab and for the slab without the metal grating are also shown for comparison purposes. The free-standing strip grating is, as expected, almost transparent along the whole explored frequency range, with a slight increase of reflectivity as frequency increases. Due to the weak interaction of the impinging wave with the metal grating, one could expect that the narrow strips only slightly disturb the reflection properties of a dielectric slab without metallic loading. This is approximately what is observed in Fig. 6 except for a sharp reflection peak located at about 56.26 GHz. The values shown as circles in the figure have been computed using

Authorized licensed use limited to: Universidad de Sevilla. Downloaded on June 03,2020 at 14:46:29 UTC from IEEE Xplore. Restrictions apply.

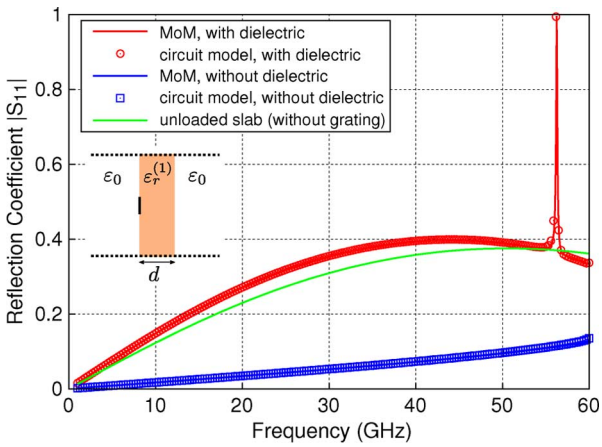

Fig. 6. Magnitude of the reflection coefficient for a strip grating printed on a dielectric slab under TM normal illumination. The reflection coefficient of the free-standing strip array and the reflection coefficient of the unloaded dielectric slab are also shown. Structure parameters: $a = 5$ mm, $w = 1$ mm, $d = 1$ mm, $\varepsilon_r^{(1)} = 2.2$.

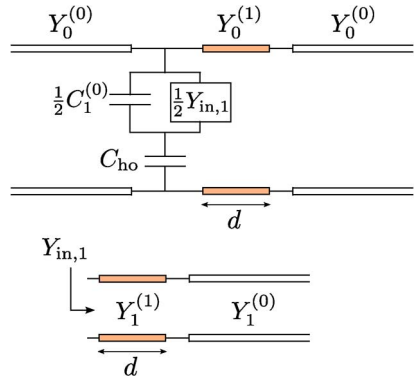

Fig. 7. Circuit model for the specific situation studied in Fig. 6.

the TM-polarization one-parameter circuit model in (27) (additionally, $N = 1$ in (27); only the first higher order frequency-dependent input admittance is explicitly considered since only that mode propagates inside the dielectric region). Note that the equivalent-circuit model accounts very accurately for the reflection spectrum of the structure.

The narrow-band reflection peak in Fig. 6 can be considered an example of extraordinary reflection [7] induced, in this case, by the presence of the dielectric slab. The circuit model also provides a simple and clear qualitative explanation of the existence of this extraordinary reflection peak. For that purpose, we consider the equivalent circuit proposed for this specific situation in Fig. 7. In this figure, $C_1^{(0)}$ is the capacitance associated with the below-cutoff first higher order mode in free space, given by

$$C_1^{(0)} = -\mathrm{j}Y_1^{(0)}/\omega. \tag{44}$$

This capacitance has a pole singularity at the cutoff frequency of the first higher order mode in free space (i.e., at the onset of the first grating lobe), $f_1^{(0)} \approx 59.96$ GHz. The input admittance of the right hand side transmission line associated with the first higher order mode is

$$Y_{\mathrm{in},1} = \mathrm{j}Y_1^{(1)} \frac{\omega C_1^{(0)} + Y_1^{(1)} \tan\left(\beta_1^{(1)} d\right)}{Y_1^{(1)} - \omega C_1^{(0)} \tan\left(\beta_1^{(1)} d\right)} \tag{45}$$

which takes into account the presence of the dielectric slab on the contribution of this specific mode. For low frequency values, at which the first higher order mode is evanescent in the dielectric region, the characteristic admittance $Y_1^{(1)}$ is capacitive (imaginary and positive), feature that is passed on to the input admittance $Y_{\mathrm{in},1}$. At the cutoff frequency of this mode in the dielectric region, $f_1^{(1)} \approx 40.42$ GHz, $Y_1^{(1)}$ has a singularity, but the wavenumber $\beta_1^{(1)}$ is zero, and the input admittance remains capacitive and finite. For frequencies above $f_1^{(1)}$, $Y_1^{(1)}$ is real and decreases as frequency increases. On the other hand, $C_1^{(0)}$ has a pole at $f_1^{(0)}$ and, therefore, at some frequency between $f_1^{(1)}$ and $f_1^{(0)}$, we will find that

$$Y_1^{(1)} = \omega C_1^{(0)} \tan\left(\beta_1^{(1)} d\right) \tag{46}$$

where the denominator of (45) becomes zero. At this frequency, the input admittance $Y_{\mathrm{in},1}$ becomes infinite, causing a short circuit that leaves only the higher order capacitance, C_{ho}, in the equivalent circuit shown in Fig. 7. For higher frequencies, the denominator in (45) reverses its sign causing that $Y_{\mathrm{in},1}$ becomes inductive. At frequencies slightly above the singularity of $Y_{\mathrm{in},1}$, this inductive input admittance is very large and dominates over $C_1^{(0)}$. However, taking into account once again that $C_1^{(0)}$ grows to infinity at $f_1^{(0)}$, it is clear that this capacitance gains relevance as frequency is further increased, which counteracts the inductive admittance $Y_{\mathrm{in},1}$ and decreases the value of the global admittance of the parallel connection between both of them. Eventually, this global inductive admittance will cancel out the higher order capacitance C_{ho}, namely,

$$\mathrm{j}\omega C_1^{(0)} + Y_{\mathrm{in},1} = \mathrm{j}\omega 2C_{\mathrm{ho}}. \tag{47}$$

When this condition is satisfied, the complete equivalent circuit in Fig. 7 acts as a resonant LC series, short-circuiting the transmission line and causing the incident wave to be totally reflected by the dielectric loaded strip grating. Note that this resonance takes place at a frequency between the divergence of the input admittance [given by condition (46)] and the onset of the first grating lobe ($f_1^{(0)} \approx 59.96$ GHz in our case).

As neither $Y_1^{(1)}$ nor $C_1^{(0)}$ depend on the thickness of the dielectric slab, d, it is clear that (46) is satisfied at a higher frequency value for smaller values of d, making the total reflection peak move closer to $f_1^{(0)}$ for thinner dielectric slabs. Also, the peak will be narrower due to the more pronounced frequency dependence of $C_1^{(0)}$. A similar shift of the reflection peak to higher frequencies is expected when the slab permittivity is decreased, due to the increase of the cutoff frequency of the first higher order mode in the slab region. All the above predictions are confirmed in Fig. 8, which shows the reflection coefficient for different values of the slab thickness and permittivity. As it can be observed, the agreement between the results provided by the circuit model and the very accurate full-wave method of moments (MoM) data is excellent in all cases. An interesting

Authorized licensed use limited to: Universidad de Sevilla. Downloaded on June 03,2020 at 14:46:29 UTC from IEEE Xplore. Restrictions apply.

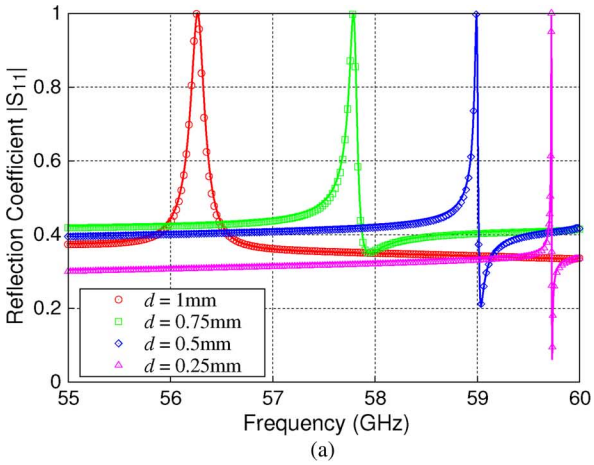

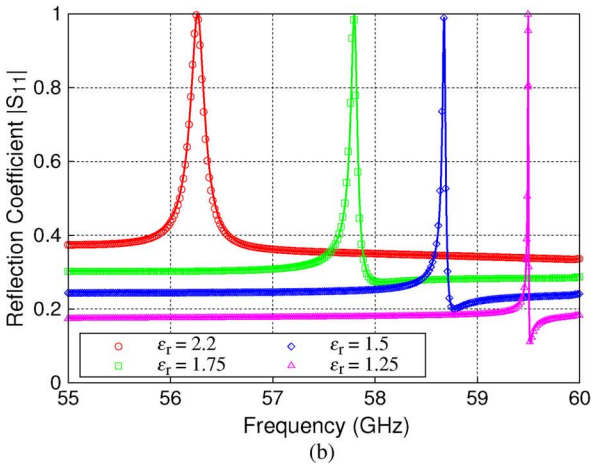

Fig. 8. Reflection coefficient of the geometry in Fig. 6 for several values of: (a) the thickness of the dielectric slab ($a = 5$ mm, $w = 1$ mm, $\varepsilon_r^{(1)} = 2.2$); and (b) the dielectric constant ($a = 5$ mm, $w = 1$ mm, $d = 1$ mm). Solid lines: results obtained using a full-wave method of moments code. Discrete points: Data provided by our equivalent circuit (27) with $N = 1$.

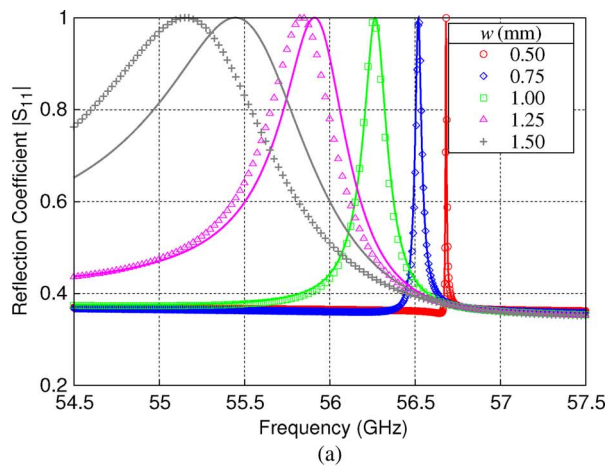

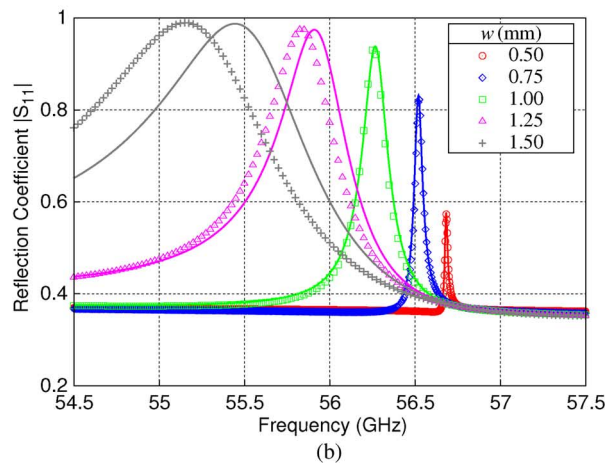

Fig. 9. Evolution of the position and bandwidth of the extraordinary reflection peak of the structure in Fig. 6 when varying the strip width w. Solid lines represent full-wave MoM results whereas the discrete points are the data obtained using our equivalent circuit (27) with $N = 1$. Structure parameters: (a) $a = 5$ mm, $d = 1$ mm, $\varepsilon_r^{(1)} = 2.2$ (same as Fig. 6). (b) Same as (a) but with a practical lossy substrate with $\tan\delta = 10^{-3}$.

feature of the reflection curves in Fig. 8(a) is that the total reflection peak is followed by a dip in the reflection coefficient (i.e., a transmission peak), which becomes more pronounced for the smallest values of d. The equivalent circuit also provides a simple explanation for this detail. The input admittance of the transmission line that models the propagation of the TEM wave to the right of the grating can be written as

$$Y_{\text{in},0} = \frac{\sqrt{\varepsilon_r^{(1)}}}{\eta_0} \frac{1 + \text{j}\sqrt{\varepsilon_r^{(1)}} \tan\left(\sqrt{\varepsilon_r^{(1)}} k_0 d\right)}{\sqrt{\varepsilon_r^{(1)}} + \text{j} \tan\left(\sqrt{\varepsilon_r^{(1)}} k_0 d\right)}. \tag{48}$$

In the electrically thin limit, $k_0 d \ll 1$, (48) can be reduced to

$$Y_{\text{in},0} = \frac{1}{\eta_0} + \text{j}\omega\varepsilon_0 \left(\varepsilon_r^{(1)} - 1\right) d \tag{49}$$

if only first-order terms are retained in the small parameter expansion. This represents a parallel connection of the free-space admittance and a small capacitance that can be interpreted as the difference between the capacitance of the short length of transmission line representing the TEM wave in the dielectric and the capacitance representing the same length in vacuum. Now, for frequencies slightly above the short circuit condition (47), the admittance of the parallel connection of $C_1^{(0)}$ and $Y_{\text{in},1}$ is of inductive nature and slightly smaller than $\text{j}\omega C_{\text{ho}}$. Then, the admittance of the complete equivalent circuit is inductive and very large. However, as $C_1^{(0)}$ quickly grows as frequency further increases (recall that this parameter has a singularity at $f_1^{(0)}$), it will compensate for the inductive admittance $Y_{\text{in},1}$, thus reducing the inductive global admittance of the complete equivalent circuit, which indeed will become zero when $\text{j}\omega C_1^{(0)} = -Y_{\text{in},1}$. During this process, the global inductive admittance of the complete equivalent circuit will eventually cancel out the capacitance introduced by the TEM input admittance in (49), giving rise to an almost perfect impedance matching (very low reflection) for very thin dielectric slabs.

Next, we study the influence of the strip width, w. This study is very important since, in principle, the proposed equivalent-circuit model is valid only in the narrow strip limit. Fig. 9(a) shows the excursion of the reflection peak for different values of w. Specifically, as the strip width increases, C_{ho} becomes larger thereby shifting the reflection peak towards lower frequencies. The figure also shows that the results provided by our

Authorized licensed use limited to: Universidad de Sevilla. Downloaded on June 03,2020 at 14:46:29 UTC from IEEE Xplore. Restrictions apply.

one-parameter circuit model start to deteriorate as the strips become wider. However, the results are excellent up to $w = 1$ mm (i.e., for $w/a \lesssim 0.2$). For $w = 1.25$ mm, the model still provides very accurate results, whereas for $w = 1.5$ mm, the deviation is more noticeable; nevertheless, the relative error in the position of the peak is less than 0.4%.

It was already mentioned that dielectric losses can be incorporated in a straightforward way in the model. Thus, Fig. 9(b) shows the same results as in Fig. 9(a) but now for a practical low-loss dielectric substrate $(\tan\delta = 10^{-3})$. The parameter of the circuit model, $C_{\rm ho}$, is obtained from the full-wave results at one single frequency value (1 GHz) *for the lossless structure*. In other words, the same value of the $C_{\rm ho}$ parameter is used in both Fig. 9(a) and (b). A slight deviation with respect to the full-wave results is observed for the wider strips, very similar to the lossless structure in Fig. 9(a). It can be observed that the decrease of the reflected power due to the presence of dielectric losses is very accurately predicted by the circuit model. As expected, the effect of losses is more significant for the narrower strips (the peaks are sharper). However, even for the narrowest considered strips $(w = 0.5$ mm), the reflection peak is still quite noticeable, and the gratings with strips of $w = 1$ mm and wider are almost unaffected by the small dielectric losses here considered.

The previous spectra were obtained for a strip grating printed on a thin low-permittivity substrate. It is clearly expected that the spectra increase their complexity for high-permittivity and/or thick substrates. Results (not included) obtained for different strip widths in the case of a high-permittivity substrate show that the range of applicability of the circuit model is slightly reduced with respect to the low-permittivity case. As a general rule, it has been found that our models provide reasonably accurate results for $w/\lambda_0 \lesssim 0.2$ and $w/a \lesssim 1/3$.

In Fig. 10, we study the performance of the equivalent-circuit model for a slit grating printed on a dielectric slab under normal TE incidence conditions. The transmission coefficient for the free-standing screen (i.e., without the dielectric slab) is also shown. As expected, the transmission is very low over most of the explored frequency band. However, the presence of the dielectric slab gives rise to a sharp transmission peak at $f \approx 56$ GHz, followed by a transmission zero (Fano-like resonance). Again, our circuit model very accurately reproduces the transmission behavior of the printed slit grating and provides a simple qualitative explanation of the observed behavior. shahb

The equivalent circuit for the configuration studied in Fig. 10 is depicted in Fig. 11, where $L_1^{(0)}$ represents the inductance associated with the below-cutoff first higher order mode in free space, which is given by

$$L_1^{(0)} = \frac{1}{{\rm j}\omega Y_1^{(0)}}. \tag{50}$$

The value of the admittance of the global higher order inductance $L_{\rm ho}$ is very high when compared with the characteristic admittances of the lines, thus explaining the overall strong reflection for most of the considered frequency range. The input admittance $Y_{{\rm in},1}$ can be written as

$$Y_{{\rm in},1} = -{\rm j}Y_1^{(1)} \frac{\frac{1}{\omega L_1^{(0)}} - Y_1^{(1)} \tan\left(\beta_1^{(1)} d\right)}{Y_1^{(1)} + \frac{1}{\omega L_1^{(0)}} \tan\left(\beta_1^{(1)} d\right)}. \tag{51}$$

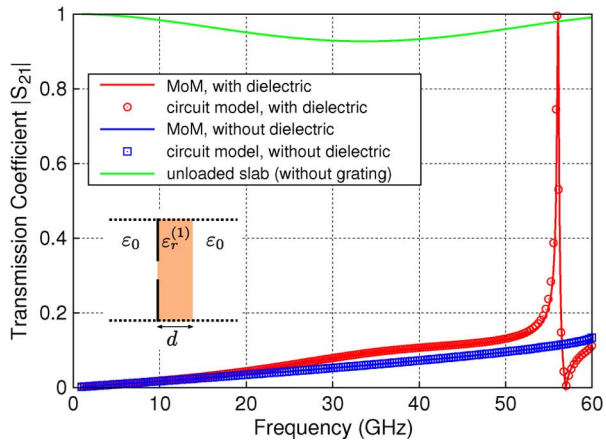

Fig. 10. Magnitude of the transmission coefficient under normal TE illumination for a slit grating with $w = 1$ mm and $a = 5$ mm printed on a dielectric substrate with thickness $d = 1.5$ mm and $\varepsilon_r^{(1)} = 2.2$. The transmission coefficient of the free-standing grating (without dielectric slab) and of the unloaded dielectric slab are also shown.

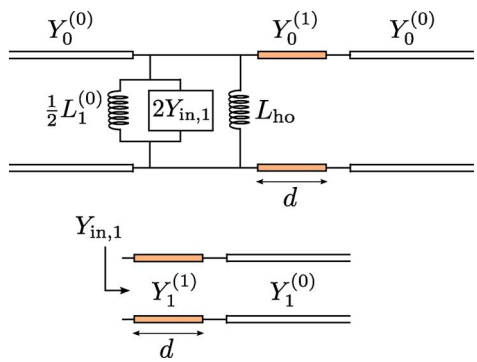

Fig. 11. Circuit model for the situation studied in Fig. 10.

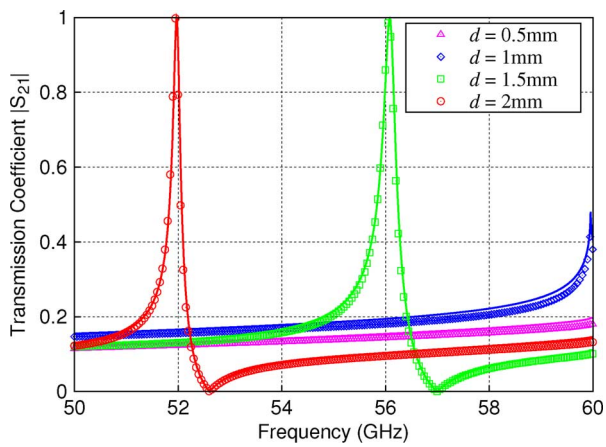

Fig. 12. Magnitude of the transmission coefficient for the same slit grating previously considered in Fig. 10, but printed on dielectric slabs with several different thicknesses and permittivity $\varepsilon_r^{(1)} = 2.2$. Solid lines: data obtained from a full-wave MoM technique. Discrete symbols: data computed from the equivalent-circuit model (19) with $N = 1$ term.

At low frequencies, this admittance is inductive. However, $L_1^{(0)}$ is singular at the onset frequency of the first grating lobe

Authorized licensed use limited to: Universidad de Sevilla. Downloaded on June 03,2020 at 14:46:29 UTC from IEEE Xplore. Restrictions apply.

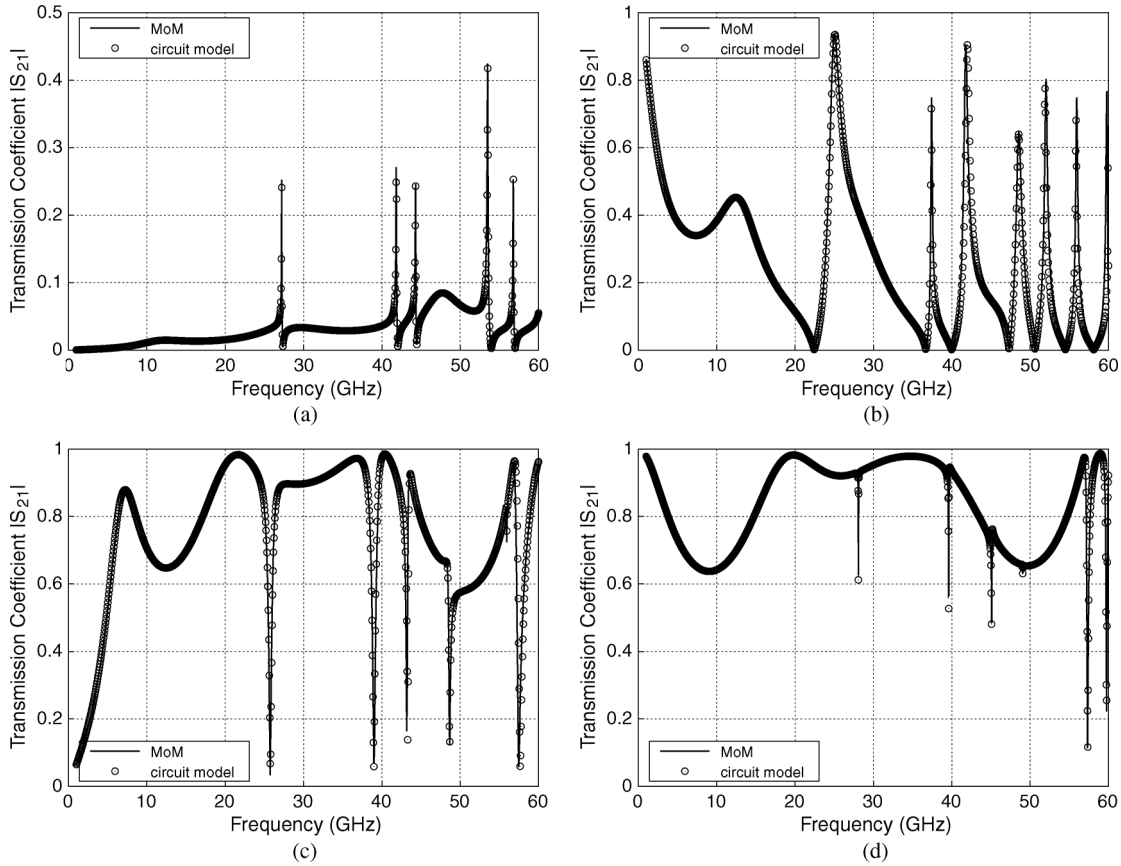

Fig. 13. Magnitude of the transmission coefficient at normal incidence. The period is $a = 5$ mm and the slit/strip width is $w = 0.5$ mm. The grating is embedded in the layered media shown in Fig. 1 with $\varepsilon_r^{(1)} = 2.2$, $\varepsilon_r^{(2)} = 10.2$, $\varepsilon_r^{(3)} = 4$, $d_1 = d_2 = d_3 = 1.5$ mm. All the dielectric layers are lossy with $\tan\delta = 0.001$. (a) Slit grating under TE illumination. (b) Slit grating under TM illumination. (c) Strip grating under TE illumination. (d) Strip grating under TM illumination.

($f_1^{(0)} \approx 59.96$ GHz). Therefore, $Y_{\mathrm{in},1}$ becomes capacitive at certain frequency below $f_1^{(0)}$ satisfying

$$\frac{1}{\omega L_1^{(0)}} = Y_1^{(1)} \tan\left(\beta_1^{(1)} d\right). \tag{52}$$

For thin substrates, this capacitive admittance is much lower than the global higher order admittance given by $1/\mathrm{j}\omega L_{\mathrm{ho}}$, and thus only strong reflection is expected for any frequency. However, if the electrical length of the transmission line corresponding to the first higher order mode inside the dielectric approaches one quarter of the dielectric wavelength ($\beta_1^{(1)} d \approx \pi/2$), then $Y_{\mathrm{in},1}$ might become significant. In fact, for those frequencies where this transmission line is slightly larger than one quarter of the wavelength, the tangent functions in (51) become negative, large and quickly decaying. Thus, the denominator of $Y_{\mathrm{in},1}$ in (51) will eventually vanish, causing this admittance to become infinite, which explains the transmission zero. Moreover, as the capacitive admittance $Y_{\mathrm{in},1}$ grows towards its divergence point, at some frequency value, it will counteract the $L_1^{(0)}$ and L_{ho} contributions to make the complete equivalent circuit behave as a resonant LC tank (open circuit). At this frequency, the slit grating does not have any effect on the impinging wave and the value of the transmission coefficient will be the same as for the dielectric slab alone, which means a considerable increase in the transmission level with respect

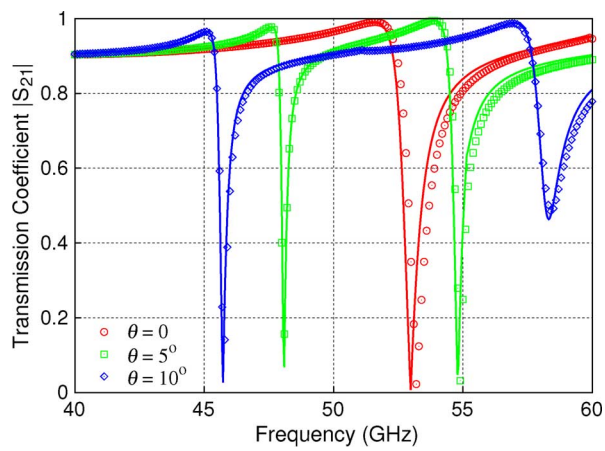

Fig. 14. Transmission coefficient for a strip-like grating under TE illumination. The strips are extremely narrow ($w = 0.25$ mm), in such a way that strong transmission is expected along the shown frequency range. However transmission zeros or dips induced by the presence of the slab are observed. Data: $a = 5$ mm, $d = 1.5$ mm, $\varepsilon_r = 2.2$.

to the situation without slab (see Fig. 10). However, the transmission peak observed in the spectrum is even higher than the expected from this reasoning. To explain this fact, it should be considered that the input admittance of the right hand side TEM transmission line given by $Y_{\mathrm{in},0}$ in (48), which is capacitive at low frequencies, has already become inductive (remind that

Authorized licensed use limited to: Universidad de Sevilla. Downloaded on June 03,2020 at 14:46:29 UTC from IEEE Xplore. Restrictions apply.

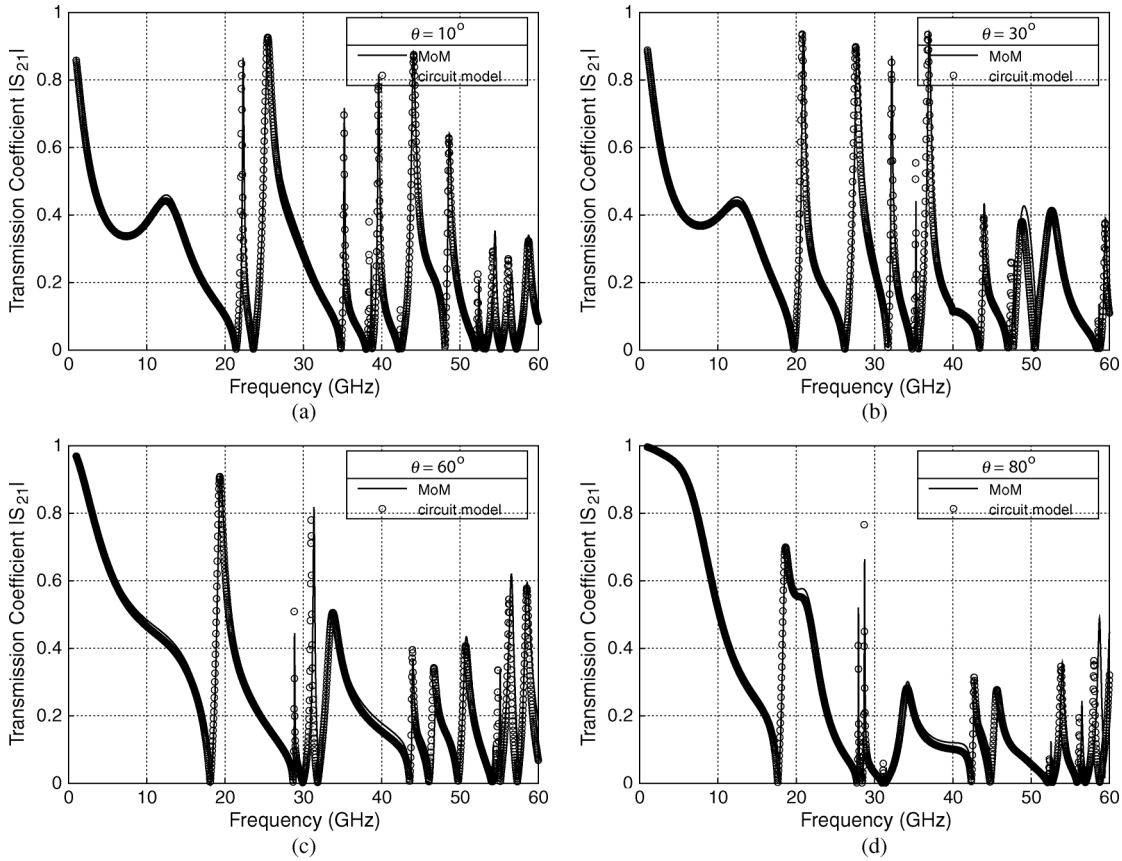

Fig. 15. Magnitude of the transmission coefficient under TM oblique incidence of a slit grating ($a = 5$ mm, $w = 0.5$ mm) embedded in the layered media shown in Fig. 1 with $\varepsilon_r^{(1)} = 2.2$, $\varepsilon_r^{(2)} = 10.2$, $\varepsilon_r^{(3)} = 4$, $d_1 = d_2 = d_3 = 1.5$ mm. All the dielectric layers are lossy with $\tan\delta = 0.001$. (a) $\theta_{\rm inc} = 10°$, (b) $\theta_{\rm inc} = 30°$, (c) $\theta_{\rm inc} = 60°$, and (d) $\theta_{\rm inc} = 80°$.

$\sqrt{\varepsilon_r^{(1)}}k_0 > \beta_1^{(1)}$, which means that the length of transmission line corresponding to the TEM mode in the dielectric is already larger than one quarter of the wavelength). In consequence, for frequencies above the LC resonance, the growing capacitive admittance of the equivalent circuit compensates the inductive part of $Y_{\rm in,0}$ and results in an even higher transmission peak. The studied phenomenon is the same reported in [19] or, more recently, in [33] and [34].

Previously, it was mentioned that the slit grating under TE illumination does not exhibit peaks of extraordinary transmission unless the electrical thickness of the substrate reaches certain threshold. This can be clearly observed in Fig. 12, where only the curves with $d > 1$ mm show total transmission peaks, in agreement with the conclusions in [33]. A study carried out (not explicitly shown) on the efficiency and range of applicability of the equivalent-circuit model yields basically the same conclusions as for the strip grating under TM polarization.

As a final example of normal incidence, Fig. 13 collects all the possible scenarios of TM/TE polarizations and strip/slit gratings. The gratings are embedded in a multilayered environment as that shown in Figs. 4 and 5, whose characteristics are detailed in the caption of Fig. 13. The multilayered nature of the structure makes the observed reflection/transmission spectra have multiple peaks and dips. However, and despite the very involved shape of the different spectra, all the situations are very accurately accounted for by our one-parameter equivalent-circuit model. It is remarkable that with the use of only one low-frequency full-wave datum, the equivalent-circuit model is able to reproduce even the extremely narrow-band details of the spectra (it should be noted that the obtaining of these narrow-band details via the full-wave method requires a very fine frequency sweeping—about 2000 frequency points in our computations to generate the curves in Fig. 13).

In order to validate our model under oblique incidence conditions Fig. 14 shows the transmission coefficient in the case of narrow strips and parallel polarization (TE) for three different incidence angles. For normal incidence, a behavior that is quasi-dual to the one reported in [19] and [33] or in Fig. 12 is observed (there is a strong narrow band transmission zero not expected in the absence of dielectric slab). This behavior can easily be explained from our circuit model. It is interesting to see how, for oblique incidence, the transmission zero splits into two dips. According to our model, it happens because of the splitting of each modal admittance into the pair of admittances associated with the corresponding spatial harmonics of positive and negative order. It should be noted that, for oblique incidence with $\theta_{\rm inc} = 5°$, the higher frequency dip is a perfect zero whereas for $\theta_{\rm inc} = 10°$ this dip no longer reaches zero. The reason for that behavior can be explained looking at the cutoff frequencies of the first higher order spatial harmonic in free space: $f_{-1}^{(0)} = 55.15$ GHz for $\theta_{\rm inc} = 5°$ and $f_{-1}^{(0)} = 51.09$ GHz for $\theta_{\rm inc} = 10°$. It can be observed that the dips are below the grating lobe regime for $\theta_{\rm inc} = 5°$, whereas the second dip for $\theta_{\rm inc} = 10°$ is already within the grating lobe regime. In this

Authorized licensed use limited to: Universidad de Sevilla. Downloaded on June 03,2020 at 14:46:29 UTC from IEEE Xplore. Restrictions apply.

latter case, the input admittance of the $n = -1$ harmonic is resistive for $f > f_{-1}^{(0)}$, thus precluding the appearance of a perfect short circuit.

In Fig. 15, it is shown a final example of oblique incidence and TM polarization for a slit-like grating embedded in a multilayered environment [this structure was already studied in Fig. 13(b) for normal incidence]. Full-wave MoM data are compared with those computed from the equivalent-circuit model for several angles of incidence (the whole spectra here considered require hundreds to thousands of evaluations of the scattering parameters when obtained from the full-wave numerical approach). This comparison shows a very good agreement in spite of the high number of peaks and dips observed in the transmission spectrum. In the present case, it is important to point out that our simple one-parameter models allow us to reproduce the spectrum even beyond the grating-lobe regime. The appearance of the grating-lobe regimes are at the following frequencies: $f_{-1}^{(0)} = 51.09$ GHz for $\theta_{\rm inc} = 10^\circ$, $f_{-1}^{(0)} = 39.97$ GHz for $\theta_{\rm inc} = 30^\circ$, $f_{-1}^{(0)} = 32.13$ GHz for $\theta_{\rm inc} = 60^\circ$, and $f_{-1}^{(0)} = 30.21$ GHz for $\theta_{\rm inc} = 80^\circ$. It is somewhat surprising that this very simple equivalent-circuit model can provide so accurately results for frequencies so high in the grating-lobe regime as that shown, for example, in Fig. 15(d).

IV. Conclusion

This paper has reported a quasi-analytical method to model strip-like and slit-like diffraction gratings printed or embedded in layered structures. The method provides different equivalent-circuit models for different polarizations and different types of structures. Each of these models allow us to reproduce the characteristics of complex reflection/transmission spectra using just one adjustable parameter, which can be computed from full-wave data generated at a single frequency point. In contrast with previously published works on the topic, the models are not restricted to the low-frequency limit or to the semi-infinite medium approximation. Recently reported phenomena such as extraordinary transmission/reflection induced by the presence of dielectric slabs are easily explained within the proposed simple circuit-theory frame. The accuracy of the quasi-analytical results is surprisingly good beyond the apparent limitation of the basic theory here developed.

References

[1] R. W. Wood, "On a remarkable case of uneven distribution of light in a diffraction grating spectrum," *Phylosoph. Mag.*, vol. 4, pp. 396–402, 1902.

[2] R. W. Wood, "Diffraction gratings with controlled groove form and abnormal distribution of intensity," *Phylosoph. Mag.*, vol. 23, pp. 310–317, 1912.

[3] L. Rayleigh, "Dynamical theory of the grating," *Proc. Roy. Soc. (London)*, vol. A79, pp. 399–416, 1907.

[4] U. Fano, "The theory of anomalous diffraction gratings and of quasi-stationary waves on metallic surfaces (Sommerfeld's waves)," *J. Opt. Soc. Amer.*, vol. 31, pp. 213–222, 1941.

[5] T. W. Ebbesen, H. J. Lezec, H. F. Ghaemi, T. Thio, and P. A. Wolff, "Extraordinary optical transmission through sub-wavelength hole arrays," *Nature*, vol. 391, pp. 667–669, Feb. 1998.

[6] C. Genet and T. W. Ebbesen, "Light in tiny holes," *Nature*, vol. 445, pp. 39–46, Jan. 2007.

[7] F. J. García-de-Abajo, "Colloquium: Light scattering by particle and hole arrays," *Rev. Modern Phys.*, vol. 79, pp. 1267–1290, Oct.–Dec. 2007.

[8] K. Y. Bliokh, Y. P. Bliokh, V. Freilikher, S. Savel'ev, and F. Nori, "Colloquium: Unusual resonators: Plasmonics, metamaterials, and random media," *Rev. Mod. Phys.*, vol. 80, pp. 1201–1213, Oct.–Dec. 2008.

[9] F. J. García-Vidal, L. Martín-Moreno, T. W. Ebbesen, and L. Kuipers, "Light passing through subwavelength apertures," *Rev. Mod. Phys.*, vol. 82, pp. 729–787, Jan.–Mar. 2010.

[10] R. Gordon, A. G. Brolo, D. Sinton, and K. L. Kavanagh, "Resonant optical transmission through hole-arrays in metal films: Physics and applications," *Laser Photon. Rev.*, vol. 4, no. 2, pp. 311–335, 2010.

[11] J. B. Pendry, L. Martín-Moreno, and F. J. Garcia-Vidal, "Mimicking surface plasmons with structured surfaces," *Science*, vol. 305, pp. 847–848, Aug. 2004.

[12] F. Medina, F. Mesa, and R. Marqués, "Extraordinary transmission through arrays of electrically small holes from a circuit theory perspective," *IEEE Trans. Microw. Theory Tech.*, vol. 56, no. 12, pp. 3108–3120, Dec. 2008.

[13] F. Medina, J. A. Ruiz-Cruz, F. Mesa, J. Rebollar, J. R. Montejo-Garai, and R. Marqués, "Experimental verification of extraordinary transmission without surface plasmons," *Appl. Phys. Lett.*, vol. 95, p. 071102, Aug. 2009.

[14] F. Medina, F. Mesa, J. A. Ruíz-Cruz, J. M. Rebollar, and J. R. Montejo-Garai, "Study of extraordinary transmission in a circular waveguide system," *IEEE Trans. Microw. Theory Tech.*, vol. 58, no. 6, pp. 1532–1542, Jun. 2010.

[15] A. G. Schuchinsky, D. E. Zelenchuk, and A. M. Lerer, "Enhanced transmission in microwave arrays of periodic sub-wavelength apertures," *J. Opt. A, Pure Appl. Opt.*, vol. 7, pp. S102–S109, 2005.

[16] M. Beruete, I. Campillo, M. Navarro-Cía, F. Falcone, and M. Sorolla, "Molding left- or right-handed metamaterials by stacked cutoff metallic hole arrays," *IEEE Trans. Antennas Propag.*, vol. 55, no. 6, pp. 1514–1521, Jun. 2007.

[17] F. Medina, F. Mesa, and D. C. Skigin, "Extraordinary transmission through arrays of slits: A circuit theory model," *IEEE Trans. Microw. Theory Tech.*, vol. 58, no. 1, pp. 105–115, Jan. 2010.

[18] V. Lomakin and E. Michielssen, "Enhanced transmission through metallic plates perforated by arrays of subwavelength holes and sandwiched between dielectric slabs," *Phys. Rev. B*, vol. 71, p. 235117.

[19] E. Moreno, L. Martín-Moreno, and F. J. García-Vidal, "Extraordinary optical transmission without plasmons: The s-polarization case," *J. Opt. A, Pure Appl. Opt.*, vol. 8, pp. S94–S97, 2006.

[20] V. Lomakin and E. Michielssen, "Beam transmission through periodic subwavelength hole structures," *IEEE Trans. Antennas Propag.*, vol. 55, no. 6, pp. 1564–1581, Jun. 2007.

[21] R. Ortuño, C. García-Meca, F. J. Rodríguez-Fortuño, J. Martí, and A. Martínez, "Multiple extraordinary optical transmission peaks from evanescent coupling in perforated metal plates surrounded by dielectrics," *Opt. Express*, vol. 18, no. 8, pp. 7893–7898, Apr. 2010.

[22] B. Munk, *Frequency Selective Surfaces: Theory and Design*. New York: Wiley, 2000.

[23] R. Ulrich, "Far-infrared properties of metallic mesh and its complementary structure," *Infrared Phys.*, vol. 7, pp. 37–55, 1967.

[24] R. Ulrich, "Effective low-pass filters for far infrared frequencies," *Infrared Phys.*, vol. 7, pp. 65–74, 1967.

[25] P. G. J. Irwin, P. A. R. Ade, S. B. Calcutt, F. W. Taylor, J. S. Seeley, R. Hunneman, and L. Walton, "Investigation of dielectric spaced resonant mesh filter designs for PMIRR," *Infrared Phys.*, vol. 34, no. 6, pp. 549–563, 1993.

[26] C. T. Cunningham, "Resonant grids and their use in the construction of submillimeter filters," *Infrared Phys.*, vol. 23, no. 4, pp. 207–215, 1983.

[27] F. Bayatpur and K. Sarabandi, "Single-layer higher-order miniaturized-element frequency-selective surfaces," *IEEE Trans. Microw, Theory Tech.*, vol. 56, no. 4, pp. 774–781, Apr. 2008.

[28] F. Bayatpur and K. Sarabandi, "Multipole spatial filters using metamaterial-based miniaturized-element frequency-selective surfaces," *IEEE Trans. Microw. Theory Tech.*, vol. 56, no. 12, pp. 2742–2747, Dec. 2008.

[29] O. Luukkonen, C. Simovski, G. Granet, G. Goussetis, D. Lioubtchenko, A. V. Risnen, and S. A. Tretyakov, "Simple and accurate analytical model of planar grids and high-impedance surfaces comprising metal strips or patches," *IEEE Trans. Antennas Propag.*, vol. 56, no. 6, pp. 1624–1632, Jun. 2008.

[30] C. S. R. Kaipa, A. B. Yakovlev, F. Medina, F. Mesa, C. A. M. Butler, and A. P. Hibbins, "Circuit modeling of the transmissivity of stacked two-dimensional metallic meshes," *Opt. Express*, vol. 18, no. 13, pp. 13309–13320, Jun. 2010.

Authorized licensed use limited to: Universidad de Sevilla. Downloaded on June 03,2020 at 14:46:29 UTC from IEEE Xplore. Restrictions apply.

[31] M. García-Vigueras, F. Mesa, F. Medina, R. Rodríguez-Berral, and J. L. Gómez-Tornero, "Equivalent circuits for conventional and extraordinary reflection in dipole arrays," presented at the Int. Microw. Symp., Baltimore, MD, Jun. 2011.
[32] R. Rodríguez-Berral, F. Medina, and F. Mesa, "Circuit model for a periodic array of slits sandwiched between two dielectric slabs," *Appl. Phys. Lett.*, vol. 96, p. 161104, Apr. 2010.
[33] M. Beruete, M. Navarro-Cía, S. A. Kuznetsov, and M. Sorolla, "Circuit approach to the minimal configuration of terahertz anomalous extraordinary transmission," *Appl. Phys. Lett.*, vol. 98, p. 014106, 2011.
[34] M. Beruete, M. Navarro-Cía, and M. Sorolla, "Understanding anomalous extraordinary transmission from equivalent circuit and grounded slab concepts," *IEEE Trans. Microw. Theory Tech.*, vol. 59, no. 9, pp. 2180–2188, Sep. 2011.
[35] M. Guglielmi and A. A. Oliner, "Multimode network description of a planar periodic metal-strip grating at a dielectric interface—Part I: Rigorous network formulations," *IEEE Trans. Microw. Theory Tech.*, vol. 37, no. 3, pp. 535–541, Mar. 1989.
[36] M. Guglielmi and A. A. Oliner, "Multimode network description of a planar periodic metal-strip grating at a dielectric interface-Part II: Small-aperture and small-obstacle solutions," *IEEE Trans. Microw. Theory Tech.*, vol. 37, no. 3, pp. 542–552, Mar. 1989.
[37] R. B. Adler, L. J. Chu, and R. M. Fano, *Electromagnetic Energy Transmission and Radiation*. London, U.K.: Chapman & Hall, 1960.
[38] J. Schwinger and D. S. Saxon, *Discontinuities in Waveguides*. New York: Gordon and Breach, 1968.
[39] L. A. Weinstein, *The Theory of Diffraction and the Factorization Method*. Boulder, CO: Golem Press, 1969.
[40] L. Lewin, *Theory of waveguides*. New York: Wiley, 1975.

Raúl Rodríguez-Berral was born in Casariche (Seville), Spain, in 1978. He received the Licenciado (M.Sc.) and Ph.D. degrees in physics from the University of Seville, Seville, Spain, in 2001 and 2008, respectively.

In January 2002, he joined the Department of Applied Physics 1, University of Seville, where he is currently an Assistant Professor. His research interests include the study of the spectrum and the excitation of periodic and nonperiodic planar structures and high-frequency circuit modeling.

Francisco Medina (M'90–SM'01–F'10) was born in Puerto Real, Cádiz, Spain, in November 1960. He received the Licenciado and Doctor degrees from the University of Seville, Seville, Spain, in 1983 and 1987 respectively, both in physics.

From 1986 to 1987, he spent the academic year with the Laboratoire de Microondes de l'ENSEEIHT, Toulouse, France. From 1985 to 1989, he was an Assistant Professor with the Department of Electronics and Electromagnetism, University of Seville, where, since 1990, he has been an Associate Professor of electromagnetism. He has been a Full Professor of electromagnetism since July 2009 and he is also currently Head of the Microwaves Group. His research interest includes analytical and numerical methods for guiding, resonant, and radiating structures, passive planar circuits, periodic structures, and the influence of anisotropic materials (including microwave ferrites) on such systems. He is also interested on artificial media modeling and design and extraordinary transmission phenomena.

Dr. Medina is on the Editorial Board of the *International Journal of RF and Microwave Computer-Aided Engineering* and is a reviewer of the IEEE TRANSACTIONS ON MICROWAVE THEORY AND TECHNIQUES and of approximately 30 other IEEE, Institution of Electrical Engineers (IEE), U.K., and American Physics Society journals. He has been a member of the Technical Programme Committees (TPC) of several international and local conferences and has organized a few conferences and workshops. He is a Fellow of the Massachusetts Institute of Technology (MIT) Electromagnetics Academy. He was the recipient of a Spanish Ministerio de Educación y Ciencia (MEC) Research Scholarship and a French Ministére de la Recherche et la Technologie Scholarship.

Francisco Mesa (M'93–SM'11) was born in Cádiz, Spain, in April 1965. He received the Licenciado and Doctor degrees in physics from the Universidad de Sevilla, Seville, Spain, in 1989 and 1991, respectively.

He is currently Professor in the Departamento de Física Aplicada 1, Universidad de Sevilla, Seville, Spain. His research interests focus on electromagnetic propagation/radiation in planar structures.

María García-Vigueras (S'09) was born in Murcia, Spain, in 1984. She received the Telecommunications Engineer degree from the Technical University of Cartagena (UPCT), Spain, in 2007, where she is currently working towards the Ph.D. degree.

In 2008, she joined the Department of Communication and Information Technologies, UPCT, as a Research Assistant. She has been a visiting Ph.D. student at Heriot-Watt University, Edinburgh, Scotland, U.K., the University of Seville, Spain, and the Queen's University in Belfast, Northern Ireland, U.K. Her research interests focus on the development of equivalent circuits to characterize periodic surfaces, with application to the analysis and design of leaky-wave antennas.

Authorized licensed use limited to: Universidad de Sevilla. Downloaded on June 03,2020 at 14:46:29 UTC from IEEE Xplore. Restrictions apply.